

Radiation Maculopathy After Proton Beam Therapy for Uveal Melanoma: Optical Coherence Tomography Angiography Alterations Influencing Visual Acuity

Alexandre Matet, Alejandra Daruich, and Leonidas Zografos

Department of Ophthalmology, University of Lausanne, Jules-Gonin Eye Hospital, Fondation Asile des Aveugles, Lausanne, Switzerland

Correspondence: Alexandre Matet, Hôpital Ophtalmique Jules-Gonin, Fondation Asile des Aveugles, Avenue de France 15, CP 5143, 1002 Lausanne, Switzerland; alexmatet@gmail.com.

Submitted: May 31, 2017

Accepted: July 4, 2017

Citation: Matet A, Daruich A, Zografos L. Radiation maculopathy after proton beam therapy for uveal melanoma: optical coherence tomography angiography alterations influencing visual acuity. *Invest Ophthalmol Vis Sci*. 2017;58:3851–3861. DOI:10.1167/iovs.17-22324

PURPOSE. To analyze microvascular and structural changes in radiation maculopathy and their influence on visual acuity (VA), using optical coherence tomography (OCT) and OCT angiography (OCTA).

METHODS. This was a retrospective analysis of consecutive patients with radiation maculopathy, 12 months or more after proton-beam irradiation for uveal melanoma, imaged with fluorescein angiography, OCT, and OCTA. Clinical parameters potentially affecting VA were recorded, including OCTA-derived metrics: foveal avascular zone (FAZ) area, vascular density, and local fractal dimension of the superficial (SCP) and deep capillary plexuses (DCP). Nonirradiated fellow eyes served as controls.

RESULTS. Ninety-three patients were included. FAZ was larger, while SCP/DCP capillary density and local fractal dimension were lower in the 35 irradiated than in the 35 fellow eyes ($P < 0.0001$). Microvascular alterations graded on fluorescein angiography (minimally damaged/disrupted/disorganized) were correlated to FAZ area and SCP/DCP density on OCTA ($P < 0.01$). By univariate analysis, worse VA was associated to macular detachment at presentation ($P = 0.024$), total macular irradiation ($P = 0.0008$), higher central macular thickness (CMT) ($P = 0.019$), higher absolute CMT variation ($P < 0.0001$), cystoid edema ($P = 0.030$), ellipsoid zone disruption ($P = 0.002$), larger FAZ ($P < 0.0001$), lower SCP ($P = 0.001$) and DCP capillary density ($P < 0.0001$), and lower SCP ($P = 0.009$) and DCP local fractal dimension ($P < 0.0001$). Two multivariate models with either capillary density or fractal dimension as covariate showed that younger age ($P = 0.014/0.017$), ellipsoid zone disruption ($P = 0.034/0.019$), larger FAZ ($P = 0.0006/0.002$), and lower DCP density ($P = 0.008$) or DCP fractal dimension ($P = 0.012$), respectively, were associated with worse VA.

CONCLUSIONS. VA of eyes with radiation maculopathy is influenced by structural and microvascular factors identified with OCTA, including FAZ area and DCP integrity.

Keywords: melanoma, optical coherence tomography, radiation damage, image analysis, microcirculation

Radiation maculopathy is a devastating cause of visual impairment in eyes irradiated for intraocular tumors,¹ the most frequent indication being uveal melanoma. Currently, proton-beam therapy allows local tumor control and eye preservation in most cases. Yet, for tumors close to or involving the macula, visual acuity may be jeopardized by the irradiation of the macular microvasculature, leading to the development of radiation maculopathy. This delayed complication presents clinically with lipid exudates and hemorrhages on fundus examination, cystoid macular edema or macular thinning in end-stage disease on optical coherence tomography (OCT), and exudative telangiectasia with disrupted vascular network and nonperfusion areas on fluorescein angiography (FA).²

OCT angiography (OCTA) is a recent noninvasive technique visualizing the macular microvasculature via flow detection. Its advantages over FA are its higher resolution and reproducibility,^{3,4} and its ability to segment capillary plexuses forming the macular microvasculature and their alterations. Since macular

capillaries are the primary site of injury in radiation maculopathy, OCTA is a powerful tool to investigate these pathologic changes. Moreover, the recent adjunction of quantitative tools to OCTA provides access to retinal microcirculatory metrics, such as foveal avascular zone (FAZ) dimensions,^{5,6} capillary density,^{7,8} and capillary network fractal dimension,⁹ at the level of both plexuses. Fractal dimension is a promising endpoint to measure vascular network disorganization in OCTA images, which has been used successfully in diabetic retinopathy^{10–12} and posterior uveitis.¹³

Ocular irradiation by I-125 plaque brachytherapy induces microvascular changes detected by OCTA.^{14,15} However, the consequences of proton-beam therapy, a major treatment modality for uveal melanoma, have not been assessed by OCTA. In this study, we investigated the spectrum of structural and microvascular alterations in radiation maculopathy after proton-beam therapy for uveal melanoma, and their respective influence on visual acuity, using OCT and OCTA.



METHODS

Study Subjects

This observational case series adhered to the tenets of the Declaration of Helsinki and was approved by the local Ethics Committee (CER-VD No. 2016-01861). Medical records, OCT, OCTA, and FA images from consecutive subjects treated by proton-beam irradiation for uveal melanoma, and presenting with radiation maculopathy from August 2015 to July 2016, were retrospectively analyzed. Clinical records included systemic (sex, age, presence of hypertension or diabetes), tumor-related (largest diameter, height, localization, and presence of macular detachment at presentation), and treatment-related data (degree of macular irradiation, time since proton-beam therapy, and intravitreal anti-vascular endothelial growth factor [VEGF] treatment). At our institution, plaque brachytherapy is performed for anteriorly located choroidal tumors (located ≥ 4 mm from the macula) of limited thickness (≤ 5 mm). In these cases, macular irradiation is very limited, and radiation maculopathy rarely develops. Therefore, only proton-beam-irradiated patients were included, to analyze the consequences of unavoidable macular irradiation. Proton-beam therapy was administered according to an individualized protocol established on the EyePlan software¹⁶ (v3.06c), after implantation of tantalum clips.

Eyes with history of other retinal disease, those that had received proton therapy less than 12 months earlier, with low-quality OCTA acquisitions (signal strength index < 40) or with severe motion artifacts, were excluded. When available, multimodal imaging acquired in the fellow nonirradiated eye, including OCTA, served as control.

Multimodal Imaging

B-mode, en face OCT and OCTA images were acquired on Angiovue RTx 100 (Optovue, Inc., Fremont, CA, USA). The correct automatic segmentation providing OCTA images of the superficial and deep plexuses was visually controlled. Central macular thickness (CMT) was measured on OCT volumes in the central subfield of an adapted Early Treatment of Diabetic Retinopathy Study (ETDRS) grid centered on the fovea.

FA was performed on Spectralis (Heidelberg Engineering, Heidelberg, Germany). Early frames (20–30 seconds after dye injection) were acquired with a 30° lens. A 20 × 20° 97-section B-mode OCT raster scan was acquired on Spectralis.

Capillary Network Density and Foveal Avascular Zone

The mean vascular density of 3 × 3-mm OCTA images centered on the fovea was obtained by using the built-in AngloAnalytics software of the RTx 100 device (v2016.1.0.26), at the level of the superficial and deep capillary plexuses.

The area of the FAZ was measured manually by two independent observers on masked OCTA images of the superficial capillary plexus, using ImageJ (v1.50c4, Wayne Rasband; <http://imagej.nih.gov/ij/>; provided in the public domain by the National Institutes of Health, Bethesda, MD, USA). Capillary vessels surrounding the FAZ were outlined by using the free contour function, to obtain the FAZ area in square millimeter (pixel-to-millimeter scale, 304:3). The mean from the two observers was retained.

Local Fractal Dimension

The local fractal dimension, based on the box-counting method, was used to assess the degree of superficial and deep

plexus disorganization on 3 × 3-mm OCTA. This method relies on the self-similarity of a vascular network at different scales. It calculates the fractal dimension, D_f , such that the number N of boxes of increasing pixel size R needed to cover a fractal object in the image follows a power-law: $D_f = \log(N)/\log(R)$. For a two-dimensional image, D_f is between 1 and 2. If the object is fractal over a limited range of box size R , this property is reflected by the local fractal dimension, $D_{f_{local}} = -d(\log(N))/d(\log(R))$, corresponding to the local slope of the D_f function for a given box size range. If the $D_{f_{local}}$ function is constant over a range of box sizes, then the image has a fractal behavior over these R values.

The local fractal dimension was estimated from the skeletonized 304 × 304-pixel .bmp image files exported by the OCTA software, by using a custom algorithm adapted from the “boxcount” program¹⁷ on Matlab (R2015b; MathWorks, Inc., Natick, MA, USA). From preliminary assessments showing that capillary networks on OCTA images presented a quasi-fractal behavior for box sizes ranging from 2^3 to 2^5 (8 × 8 to 32 × 32 pixels), the local fractal dimension was calculated as the mean value of the $D_{f_{local}}$ function over 2^3 -to- 2^5 -pixel boxes in each OCTA image. Illustrations of the pixel grids used to calculate the local fractal dimension of skeletonized OCTA images are provided in Figures 1 and 2.

Grading of Abnormal Features

Early-frame 30° fluorescein angiograms and OCTA images of the superficial and deep capillary plexuses were classified into three categories after qualitative evaluation of the macular microvasculature: minimally damaged (absent or minimal alterations), disrupted (focal interruptions of the perifoveal capillary ring), and disorganized (diffuse or multifocal capillary depletion).

OCT raster scans acquired on Spectralis were used to assess the presence of intraretinal cysts and ellipsoid zone disruption.

All OCT, FA, and OCTA gradings were performed by two independent observers (AM, AD). In case of discrepancy, images were adjudicated by the senior investigator (LZ).

Statistical Analyses

Analyses were performed on Prism (version 5.0f; GraphPad Software, La Jolla, CA, USA), using the Wilcoxon test for paired comparisons, Pearson coefficients for correlations, χ^2 , or Fisher's test for contingency analysis, where appropriate. Interobserver agreement was estimated with the weighted Cohen's κ for FA, OCT, and OCTA gradings, and the intraclass correlation coefficient (ICC) for FAZ measurements, using the “irr” package¹⁸ on R (v3.3.0 [2016]; R Foundation for Statistical Computing, Vienna, Austria). Clinical factors potentially influencing best-corrected visual acuity (BCVA) were investigated by using uni- and multivariate linear regression followed by stepwise forward regression, using the “MASS” package¹⁹ on R. Variables with significance level $\leq .2$ in the univariate analysis, without strong correlation with each other (Pearson $r < 0.5$), were computed into the multivariate model. The logarithm of the minimal angle of resolution (logMAR) was used for BCVA calculations. For descriptive purposes, BCVA was categorized into discrete levels ($\leq 20/200$, 20/125–20/50, and $\geq 20/40$). P values < 0.05 were considered significant.

RESULTS

Of 117 patients diagnosed with radiation maculopathy after receiving proton-beam irradiation for uveal melanoma, 14 were excluded owing to low OCTA image quality. The 93 included

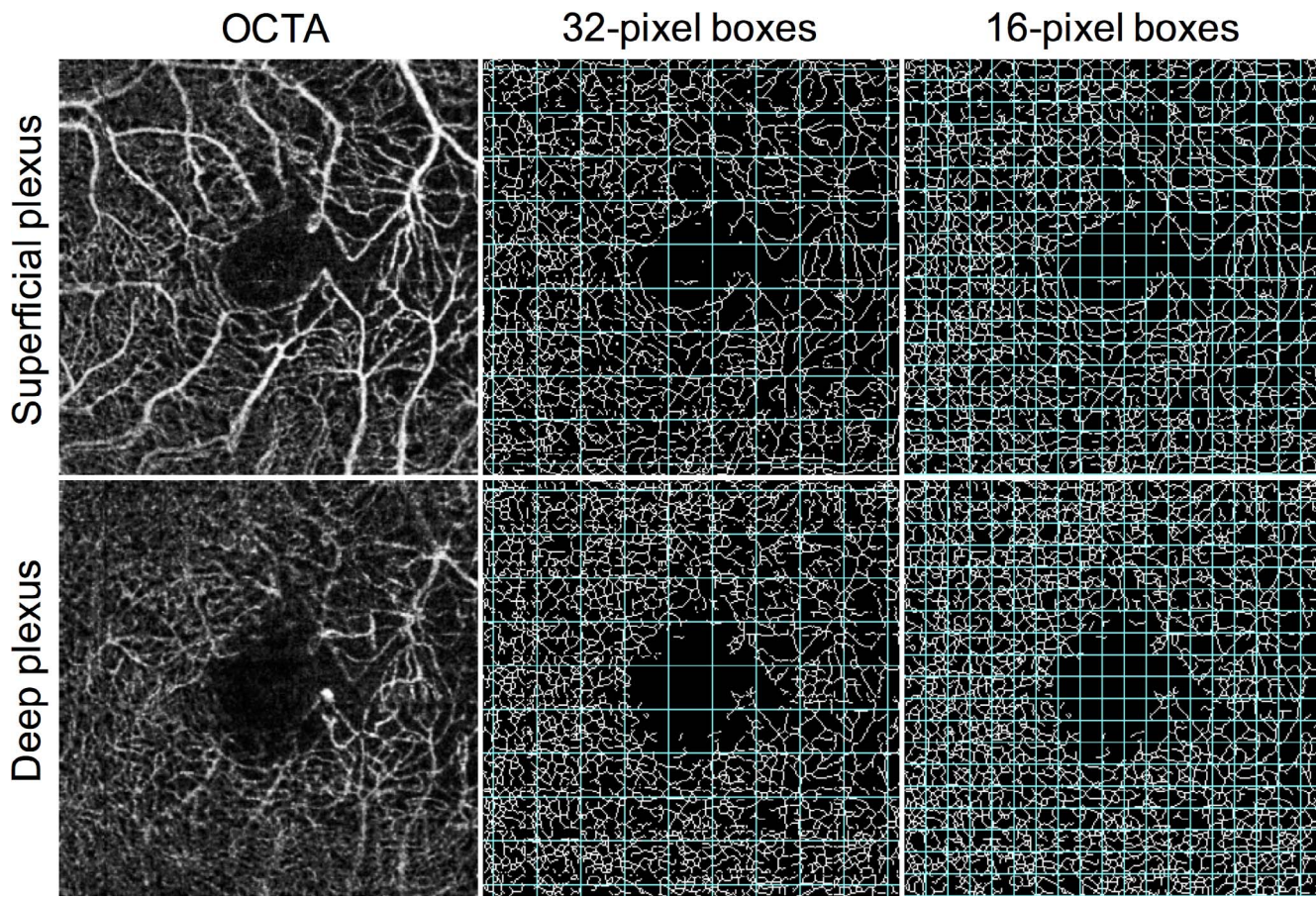


FIGURE 1. Determination of the local fractal dimension in optical coherence tomography images of a 49-year-old woman with moderately severe radiation maculopathy following proton-beam therapy for uveal melanoma. Best-corrected visual acuity was 20/30. The box-counting method was applied to the superficial (*top*) and deep (*bottom*) capillary plexuses. *Top* and *bottom left*, Original optical coherence tomography angiography images were skeletonized and superimposed with boxes of decreasing size: 32 pixels (*top* and *bottom middle*) and 16 pixels (*top* and *bottom right*), and 8 pixels (not shown). The number N of 32-, 16-, and 8-pixel boxes required to cover the vascular network was counted, and the local fractal dimension was estimated as the mean value of $-d(\log(N))/d(\log(R))$, where R is the box size in pixels. In this case, the local fractal dimension was 1.879 and 1.880 in the superficial and deep plexus, respectively.

patients (50 women, 43 men; mean age: 61.4 ± 12 years [33–84 years]) presented a broad dispersion of BCVA levels in their irradiated eye, from hand motion to 20/20. BCVA was $\leq 20/200$ in 33 eyes (36%), between 20/125 and 20/50 in 41 eyes (44%), and $\geq 20/40$ in 19 eyes (20%). Mean duration since proton-beam treatment was 3.8 ± 2.7 years (range, 1–15 years). According to treatment plans, all eyes received a collateral macular irradiation ≥ 20 Gy, and 43 eyes (46%) with posteriorly located melanomas received a full-dose macular irradiation. Clinical characteristics according to BCVA levels and overall descriptive characteristics are reported in Table 1 and Supplementary Table 1, respectively.

OCTA examination of the fellow eye was available in 35 subjects. OCTA-derived indicators of the macular microvasculature integrity in irradiated and nonirradiated fellow eyes are reported in Table 2. The FAZ was larger in irradiated than in fellow eyes ($P < 0.0001$). Similarly, capillary density and capillary network local fractal dimension of the superficial and deep plexuses were lower in irradiated than in nonirradiated eyes ($P < 0.0001$).

There was substantial agreement between raters for the qualitative grading of microvascular abnormalities on FA ($\kappa = 0.63$) and OCTA ($\kappa = 0.66$ and 0.65 for the superficial and deep plexus, respectively). There was an excellent agreement for the FAZ area ($ICC = 0.99$), and for the detection of intraretinal

cysts ($\kappa = 0.94$) and ellipsoid zone disruption on OCT ($\kappa = 0.86$).

Figure 3 illustrates the spectrum of structural and microvascular alterations observed in eyes with radiation maculopathy when using OCT, FA, and OCTA. The SCP and DCP imaged by OCTA were graded as minimally damaged in 35 and 16 eyes, disrupted in 42 and 47 eyes, and disorganized in 16 and 30 eyes, respectively. According to these categories, alterations were more severe in the deep than the superficial plexus ($P = 0.003$). In 34 eyes (37%), alterations in the deep plexus were more severely graded than in the superficial plexus, while the inverse occurred in only five cases (5%) ($P < 0.0001$).

OCT and OCTA findings according to BCVA levels are reported in Table 3. Since CMT may be abnormally increased or decreased in eyes with radiation maculopathy, depending on the presence of macular edema or thinning, the absolute change in CMT from the mean value observed in the 35 nonirradiated fellow eyes (261 μm) was considered as a clinical variable in the analysis.

A correlation analysis between OCTA-derived parameters revealed that qualitative grading (minimally damaged, disrupted, disorganized), vascular density, and local fractal dimension were positively correlated with each other in the SCP and DCP, and between both plexuses ($P < 0.009$). The correlation was strongest between vascular density and local fractal dimension

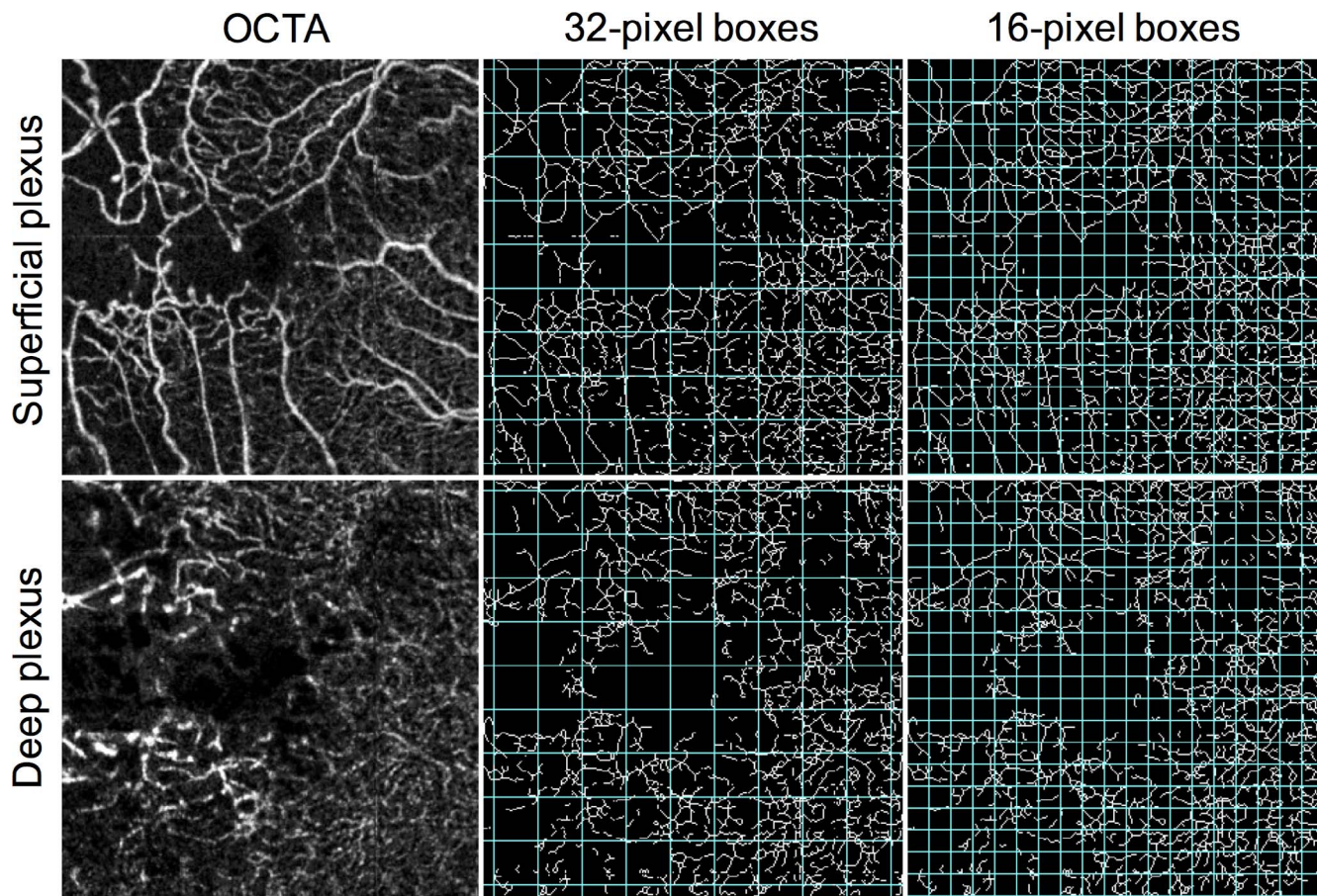


FIGURE 2. Determination of the local fractal dimension of optical coherence tomography images of a 70-year old man with severe radiation maculopathy following proton-beam therapy for uveal melanoma. Best-corrected visual acuity was 20/100. The box-counting method was applied to the superficial (*top*) and deep (*bottom*) capillary plexuses. *Top* and *bottom left*, Original optical coherence tomography angiography images were skeletonized and superimposed with boxes of decreasing size: 32 pixels (*top* and *bottom middle*), 16 pixels (*top* and *bottom right*), and 8 pixels (not shown). The number N of 32-, 16-, and 8-pixel boxes required to cover the vascular network was counted, and the local fractal dimension was estimated as the mean value of $-d(\log(N))/d(\log(R))$, where R is the box size in pixels. In this case, the local fractal dimension was 1.862 and 1.862 in the superficial and the deep plexus, respectively, lower than in the less severe case shown in Figure 1.

within each capillary plexus (Pearson $r = 0.79$ and 0.74 in the superficial and deep plexuses, respectively). CMT and CMT absolute change on OCT were correlated to vascular density ($P < 0.022$) and local fractal dimension ($P < 0.0001$) in the deep plexus, but not the superficial plexus. The FAZ area was correlated with all OCT- and OCTA-derived metrics ($P < 0.015$ and $P < 0.009$, respectively). Finally, the qualitative grading of

microvascular alteration on FA was correlated with CMT absolute change ($P < 0.0001$) and all OCTA-derived metrics ($P < 0.01$), except local fractal dimension. The detailed correlation matrix is reported in Table 4.

A series of uni- and multivariate analyses were conducted to investigate the influence of clinical and imaging parameters on BCVA. Results are reported in Table 5. Among clinical factors,

TABLE 1. Clinical and Multimodal Imaging Characteristics According to the Final Visual Acuity in 93 Patients Who Underwent Proton-Beam Therapy for Uveal Melanoma

Final BCVA, Snellen	$\leq 20/200$ (<i>n</i> = 33)	20/125–20/50 (<i>n</i> = 41)	$\geq 20/40$ (<i>n</i> = 19)
Sex, male/female, No.	18/15	19/22	6/13
Age, y	55.7 ± 11.4	65.4 ± 10.3	62.5 ± 13.1
Tumor height, mm	4.9 ± 2.0	4.6 ± 1.8	4.0 ± 1.3
Tumor distance to the fovea, disc diameter	1.0 ± 1.1	1.7 ± 1.1	1.8 ± 1.0
Macular detachment at presentation, No. (%)	26 (79)	25 (61)	7 (37)
Total macular irradiation, No. (%)	23 (70)	17 (41)	3 (16)
Time since irradiation, y	3.8 ± 2.7	4.0 ± 3.2	3.2 ± 1.2
Treatment by intravitreal anti-VEGF, No. (%)	9 (27)	18 (44)	7 (37)
Hypertension	13 (39%)	17 (41%)	6 (32%)
Diabetes	2 (6%)	4 (10%)	2 (11%)

Continuous quantitative values are reported as mean \pm standard deviation.

TABLE 2. Comparison of Optical Coherence Tomography Angiography-Derived Metrics of the Parafoveal Microvasculature Between 35 Eyes Treated With Proton-Beam Therapy for Uveal Melanoma, and Their Nonirradiated Fellow Eyes

OCTA Parameter	Irradiated Eyes (<i>n</i> = 35)	Nonirradiated Fellow Eyes (<i>n</i> = 35)	P Value†
Foveal avascular zone area,* × 10 ⁻³ mm ²	1.373 ± 1.84 (0.139–7.125)	0.266 ± 0.113 (0.022–0.522)	<0.0001
Capillary density			
Superficial plexus	39.56 ± 5.23 (29.89–51.17)	52.67 ± 2.42 (48.87–58.19)	<0.0001
Deep plexus	45.19 ± 6.69 (23.43–58.41)	58.69 ± 2.23 (52.83–62.75)	<0.0001
Local fractal dimension			
Superficial plexus	1.828 ± 0.046 (1.715–1.896)	1.908 ± .007 (1.893–1.921)	<0.0001
Deep plexus	1.819 ± 0.099 (1.353–1.900)	1.902 ± .008 (1.885–1.924)	<0.0001

Values are provided as mean ± standard deviation (range).

* Measured at the level of the superficial capillary plexus.

† Wilcoxon paired signed-rank test.

the univariate analysis identified macular detachment at presentation ($P = 0.024$), tumor distance to the fovea ($P = 0.001$), and total macular irradiation ($P = 0.0008$) as associated with worse BCVA levels, while older age was near significantly associated with better BCVA levels ($P = 0.068$). Among imaging factors, higher CMT ($P = 0.019$), higher absolute CMT change ($P < 0.0001$), presence of intraretinal cystoid edema ($P = 0.030$) or ellipsoid zone disruption ($P = 0.002$), larger FAZ area ($P < 0.0001$), lower superficial ($P = 0.001$) and deep capillary density ($P < 0.0001$), and lower superficial ($P = 0.009$) and deep local fractal dimension ($P < 0.0001$) were all associated with worse BCVA levels. Since vascular density and local fractal dimension were strongly correlated in the superficial and deep plexuses (Pearson $r = 0.79$ and 0.74, respectively; Table 4), and therefore could not be entered simultaneously in a multivariate model, two separate models were computed with either vascular density or local fractal dimension as covariate. In the first model, younger age ($P = 0.014$), presence of ellipsoid zone disruption ($P = 0.034$), larger FAZ area ($P = 0.0006$), and lower deep plexus vascular density ($P = 0.008$) were associated with worse BCVA levels (adjusted $R^2 = 0.44$). The second model yielded similar results, with younger age ($P = 0.017$), presence of ellipsoid zone disruption ($P = 0.019$), larger FAZ area ($P = 0.002$), and lower deep plexus local fractal dimension ($P = 0.012$) associated with worse BCVA levels (adjusted $R^2 = 0.43$). In both models, neither tumor distance to the fovea nor total macular irradiation had a significant influence on BCVA.

DISCUSSION

These results illustrate the variable alterations affecting the macula and its vasculature after proton-beam therapy for uveal melanoma, and how they influence visual function. All investigated OCTA-derived metrics were altered in irradiated eyes, as compared to fellow eyes. Visual acuity was independently influenced by larger FAZ area, lower deep plexus vascular density, and lower deep plexus local fractal dimension. Younger age and presence of ellipsoid zone disruption were also independently associated with worse vision. Moreover, tumor proximity to the fovea and total macular irradiation had a negative influence on visual acuity in the univariate, but not in the multivariate analysis, showing the unpredictable course of radiation maculopathy with respect to tumor- and treatment-related characteristics. Accordingly, Patel et al.²⁰ have reported that a proportion of eyes with uveal melanoma involving the fovea maintain good vision despite macular irradiation.

Signs of radiation maculopathy on fundus examination are detected in up to 89% of eyes with uveal melanoma within 3 years of proton-beam treatment.²¹ Macular irradiation and

diabetes²¹ are recognized as risk factors for radiation maculopathy. In uveal melanoma involving the fovea, smaller tumors and better baseline BCVA are identified as independent factors of better visual outcome.²⁰

OCTA is particularly suitable to image microvascular changes such as capillary nonperfusion, telangiectasia, and FAZ alterations, hallmarks of radiation maculopathy.^{21–24} However, no study has yet evaluated OCTA changes after proton-beam therapy, and their relationship with visual function. After plaque brachytherapy, Veverka et al.¹⁵ describe gradual alterations of the macular microvasculature on OCTA. Shields et al.¹⁴ have reported a decreased capillary density in both plexuses, as well as FAZ enlargement. Finally, Say et al.²⁵ have reported decreased capillary density in irradiated eyes without clinically patent maculopathy.

In the present study, we identified a relationship between radiation-induced microvascular changes on OCTA and visual function, using three different endpoints: FAZ area, automated built-in vascular density, and custom local fractal dimension of the vascular network. These endpoints reflect macular capillary network disorganization and consistently showed some degree of correlation with each other. The multivariate analysis confirmed that FAZ, deep plexus capillary density, and deep plexus local fractal dimension were associated with visual acuity. Noticeably, an observer-dependent grading of capillary network integrity was correlated to these morphologic parameters, illustrating the relevance of a clinical grading system based on OCTA in radiation maculopathy, as previously proposed.¹⁵

Although no study has yet compared vascular changes on OCTA following brachytherapy and proton-beam irradiation, a qualitative comparison of our findings with the detailed characteristics reported by Shields et al.¹⁴ shows a comparable FAZ enlargement (1.12 vs. 1.25 mm²), after similar mean duration since irradiation (45.1 vs. 46 months). Authors have also reported vascular densities based on a custom method before it became standardized in OCTA devices, which prevents reliable comparison. Therefore, additional studies evaluating both modalities with standardized OCTA metrics are needed to compare their impact on retinal plexuses, and potentially identify predictive biomarkers of treatment outcome.

Interestingly, comparable results have been reported in other disorders presenting perifoveal capillary dropout. FAZ enlargement is related to worse vision in diabetic retinopathy and retinal vein occlusions.^{26,27} Capillary density of both plexuses is correlated to visual loss in diabetic retinopathy,²⁸ branch retinal vein occlusion,^{29,30} and idiopathic macular telangiectasia type 1 (MacTel1).³¹ In addition, several investigators have shown that decreased perfusion is more frequent

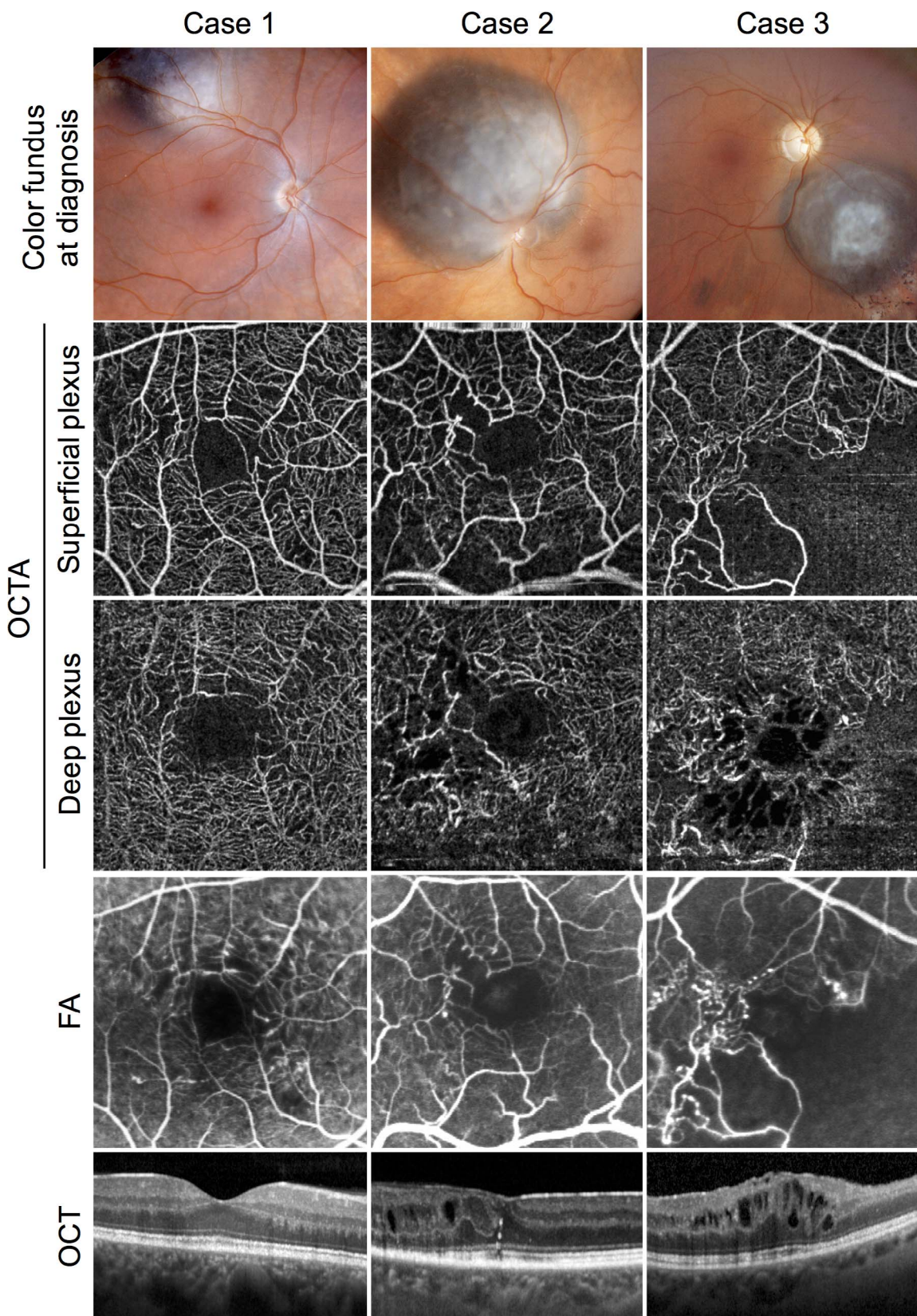


FIGURE 3. Spectrum of microvascular alterations in radiation maculopathy following proton-beam therapy for uveal melanoma visualized by multimodal imaging. Color fundus photograph at tumor diagnosis showing its localization with respect to the macula (upper line). Optical coherence tomography angiography of the superficial (second line) and deep (third line) capillary plexuses. Fluorescein angiogram 30 to 50 seconds after dye injection (fourth line) and horizontal foveal optical coherence tomography scan (lower line). Radiation maculopathy of variable severity was diagnosed in three subjects: a 47-year old man with minimally damaged superficial and deep plexuses (left column, case 1), a 67-year old man with disrupted superficial and deep plexuses (middle column, case 2), and a 63-year old woman with disorganized superficial and deep plexuses (right column, case 3).

TABLE 3. Optical Coherence Tomography and Optical Coherence Tomography Angiography Characteristics According to the Final Visual Acuity in 93 Patients Who Underwent Proton-Beam Therapy for Uveal Melanoma

Final BCVA, Snellen	$\leq 20/200$ (n = 33)	20/125–20/50 (n = 41)	$\geq 20/40$ (n = 19)
Central macular thickness, μm	323 ± 186	309 ± 104	286 ± 63
Central macular thickness absolute change,* μm	137 ± 140	81 ± 80	46 ± 49
Intraretinal cysts, No. (%)	19 (58)	20 (49)	6 (32)
Ellipsoid zone disruption, No. (%)	27 (82)	26 (63)	7 (37)
Foveal avascular zone area, [†] mm^2	2.038 ± 1.953	0.697 ± 0.730	0.470 ± 0.505
SCP qualitative grading, No. (%)			
Minimally damaged	6 (18)	16 (39)	13 (68)
Disrupted	13 (39)	23 (56)	6 (32)
Disorganized	14 (43)	2 (5)	0 (0)
DCP qualitative grading, No. (%)			
Minimally damaged	2 (6)	3 (7)	11 (58)
Disrupted	7 (21)	32 (78)	8 (42)
Disorganized	24 (72)	6 (15)	0 (0)
SCP capillary density	37.0 ± 3.8	39.0 ± 4.8	42.8 ± 6.0
DCP capillary density	42.6 ± 6.7	44.8 ± 5.5	49.8 ± 4.9
SCP local fractal dimension	1.804 ± 0.047	1.817 ± 0.050	1.851 ± 0.048
DCP local fractal dimension	1.790 ± 0.106	1.827 ± 0.055	1.856 ± 0.042

Continuous quantitative values are reported as mean \pm standard deviation.

* Compared to a reference thickness of 261 μm , observed in 35 nonirradiated fellow eyes.

† Measured at the level of the superficial capillary plexus.

in the deep than superficial plexus, in central or branch vein occlusion,^{32–34} diabetic retinopathy,³⁵ and MacTel1.³⁶ In resolved branch retinal vein occlusion, deep plexus nonperfusion has recently been identified as a more critical determinant of BCVA than superficial plexus nonperfusion.³⁰ Noticeably, vascular and structural alterations of radiation maculopathy present similarities with diabetic retinopathy, retinal vein occlusion, or MacTel1, including macular edema, microaneurysms, and capillary nonperfusion.

In the present study, OCTA revealed that the deep plexus of irradiated eyes was more severely altered than the superficial plexus. Consistently, Spaide³⁶ has reported one case of radiation maculopathy, using volume-rendering display, that showed alterations of both plexuses in the irradiated area, and adjacent areas of deep plexus nonperfusion colocalizing with macular edema. A similar pattern is visible in Figure 3, case 3. Whether deep plexus disruption is a cause or consequence of macular edema is not elucidated. Deep plexus alterations may impede the intake of interstitial fluid flow from the superficial to the deep plexus, leading to intraretinal fluid accumulation.³⁶ Deep plexus disruption could also result from tissue displacement by cystoid edema cavities, but the possibility of small interconnected capillaries forming this plexus to be stretched by edema is unlikely.^{35,36} Finally, it could also result from shadowing or edema-related signal artifacts.^{33,36,37} Here, the causal relationship between edema formation and deep plexus alteration was possibly indicated by the stronger correlation of CMT (and CMT change) with deep plexus changes, assessed by grading, vascular density, and local fractal dimension, than with superficial plexus changes (see Table 4). Importantly, this effect was controlled after statistical adjustment in the multivariate analysis, indicating that deep plexus abnormalities influence visual acuity independently from the presence of edema.

Several hypotheses could explain the greater radiosensitivity of deep plexus than superficial plexus capillaries. Microvascular radiation injury generates endothelial cell loss by impairing cell division, leading to progressive capillary closure and delayed-onset microangiopathy. This cytotoxic effect

results from “direct” DNA damage by radiation, which impairs cell division, and “indirect” free radical generation, which in turn induces DNA alterations.³⁸ Although endothelial cell turnover is slow,³⁹ an increasing fraction of endothelial cell population enters mitosis over the months following irradiation, triggering foci of endothelial damage and leading to microangiopathy.⁴⁰ Radiation-induced injury to retinal capillaries may also depend on other mechanisms than cell cycle disruption. The smaller-caliber deep plexus capillaries are more vulnerable to obturation by endothelial cell swelling, than larger superficial capillaries. Consistently, smaller capillaries are more radiosensitive than larger ones.⁴¹ Another possibility would be the different nature of endothelial cells in the deep plexus, where capillaries form an interconnected, short-segment meshwork drained by small vortices.⁴² In addition, the deep plexus is mainly composed of capillaries, unlike the superficial plexus formed by gradually smaller arterioles, capillaries, and progressively larger venules. Finally, deep plexus flow derives exclusively from the superficial plexus, so that deep plexus endothelial cells may receive a greater amount of downstream inflammatory or apoptotic signaling molecules from the upstream part of the superficial plexus after irradiation.

This study also identified younger age as an independent factor of worse visual outcomes in radiation maculopathy. Younger age has already been recognized as an independent risk factor for radiation maculopathy after plaque brachytherapy,⁴³ although this finding remains controversial.⁴⁴ As detailed above, radio-induced endothelial damage mostly results from apoptosis during cell division. Yet, endothelial cells become less proliferative with older age, undergoing fewer cellular divisions over time and ultimately not proliferating, a state called replicative senescence.^{45,46} This effect of aging may explain the greater radiosensitivity of the macular microvasculature in younger subjects.

Ellipsoid zone disruption, indicating photoreceptor damage, was associated with worse visual outcomes after irradiation. Consistently, photoreceptor damage may result from long-standing macular edema, as observed here. Several factors not

TABLE 4. Correlation Between Multimodal Imaging Methods Assessing the Parafoveal Microvasculature in 93 Eyes Treated by Proton-Beam Therapy for Uveal Melanoma

	OCT				OCTA				
P Value (Pearson r^*)	Central Macular Thickness	Central Macular Thickness	Foveal Avascular Zone Area \S	SCP Grading	DCP Grading	SCP Vascular Density	DCP Vascular Density	SCP Local Fractal Dimension	DCP Local Fractal Dimension
FA	Degree of microvascular damage \dagger	0.39 <0.0001 ($r = 0.09$)	0.007 ($r = 0.42$) <0.0001 ($r = 0.54$)	0.010 ($r = 0.27$) 0.004 ($r = -0.28$)	0.001 ($r = -0.30$)	0.67	0.67	0.39	
OCT	Central macular thickness	<0.0001 ($r = 0.83$)	0.015 ($r = 0.25$)	0.24	0.005 ($r = 0.29$)	0.53	0.022 ($r = -0.24$)	0.56	<0.0001 ($r = -0.49$)
	Central macular thickness change \ddagger	<0.0001 ($r = 0.09$)	0.003 ($r = 0.30$)	0.0002 ($r = 0.38$)	0.66	0.001 ($r = -0.33$)	0.14	<0.0001 ($r = -0.56$)	
OCTA	Foveal avascular zone area \S	<0.0001 ($r = 0.54$) <0.0001 ($r = 0.40$) 0.008 ($r = -0.27$)	<0.0001 ($r = -0.27$)	0.009 ($r = -0.27$)	0.005 ($r = -0.27$)	0.005 ($r = -0.29$)	0.001 ($r = -0.34$)		
	SCP grading	<0.0001 ($r = 0.57$) 0.002 ($r = -0.32$) 0.002 ($r = -0.31$)	0.002 ($r = -0.32$) <0.0001 ($r = 0.62$)	<0.0001 ($r = -0.40$) 0.0004 ($r = -0.36$) <0.0001 ($r = 0.62$)	0.003 ($r = -0.40$) 0.003 ($r = -0.36$) <0.0001 ($r = 0.79$)	0.003 ($r = -0.30$) 0.003 ($r = -0.31$) <0.0001 ($r = 0.79$)	0.0003 ($r = -0.30$) 0.0003 ($r = -0.31$) 0.001 ($r = 0.35$)		
	DCP grading								
	SCP vascular density								
	DCP vascular density								
	SCP local fractal dimension								

 $*$ Pearson r values are reported if $P < 0.05$. \dagger Graded as minimal, moderate, or severe. \ddagger Compared to a reference thickness of 261 μm , observed in 35 nonirradiated fellow eyes. \S Measured on optical coherence tomography images of the superficial capillary plexus.

|| Graded as minimally damaged, disrupted, or disorganized.

TABLE 5. Factors Influencing Best-Corrected Visual Acuity in 93 Patients Who Underwent Proton-Beam Therapy for Uveal Melanoma, Assessed by Univariate Analysis

	Multivariate					
	Univariate		Model 1 With Capillary Density		Model 2 With Local Fractal Dimension	
	Coefficient (Standard Error)	P Value‡	Coefficient (Standard Error)	P Value§	Coefficient (Standard Error)	P Value§
Clinical parameters						
Male sex	0.18 (0.12)	0.14	-	-	-	-
Age, by 10-y intervals	-0.09 (0.05)	0.068	-0.11 (0.04)	0.014	-0.11 (0.04)	0.017
Hypertension	0.06 (0.13)	0.63	-	-	-	-
Diabetes	-0.19 (0.22)	0.40	-	-	-	-
Tumor height > 5 mm	0.17 (0.13)	0.18	-	-	-	-
Tumor distance to fovea, DD	-0.18 (0.05)	0.001	-	-	-	-
Macular detachment at presentation	0.29 (0.13)	0.024	-	-	-	-
Total macular irradiation	0.47 (0.13)	0.0008	-	-	-	-
Time since irradiation, by 1-y intervals	0.02 (0.02)	0.38	-	-	-	-
OCT and OCTA parameters						
Central macular thickness, by 50 µm	0.05 (0.02)	0.019	-	-	-	-
Central macular thickness absolute change,* by 10-µm intervals	0.03 (0.01)	<0.0001	-	-	-	-
Intraretinal cysts	0.27 (0.12)	0.030	-	-	-	-
Ellipsoid zone disruption	0.40 (0.12)	0.002	0.26 (0.12)	0.034	0.30 (0.12)	0.019
Foveal avascular zone area†	0.22 (0.04)	<0.0001	0.13 (0.04)	0.0006	0.13 (0.04)	0.002
Capillary density, SCP	-0.04 (0.01)	0.001	-	-	x	x
Capillary density, DCP	-0.04 (-0.01)	<0.0001	-0.03 (0.01)	0.008	x	x
Local fractal dimension, SCP	-3.18 (1.19)	0.009	x	x	-	-
Local fractal dimension, DCP	-3.19 (0.72)	<0.0001	x	x	-1.81 (0.71)	0.012

Visual outcome was represented by visual acuity converted to the logarithm of minimal angle of resolution. DD, disc diameter.

* Compared to a reference thickness of 261 µm, observed in 35 nonirradiated fellow eyes.

† Measured at the level of the superficial capillary plexus.

‡ Univariate linear regression, with best-corrected visual acuity as outcome (logarithm of the minimum angle of resolution).

§ Multivariate generalized linear model, with best-corrected visual acuity as outcome (logarithm of the minimum angle of resolution). Capillary density and local fractal dimension of both plexuses were computed in two separate models owing to their strong correlation. Adjusted $R^2 = 0.44$ (model 1) and 0.43 (model 2).

influencing the visual outcome were also identified. Treatment by anti-VEGF did not modify the visual outcome because at the time of OCTA examination it had been administered mostly as prophylaxis to reduce the risk of secondary neovascularization, as previously reported.⁴⁷ The few number of eyes that received anti-VEGF because of macular edema had lower BCVA, inducing a selection bias. Recent data suggest that prophylactic bimonthly anti-VEGF therapy may contribute to vision retention after proton-beam therapy for tumors close to the macula.⁴⁸ Further studies are needed to address the exact effect of anti-VEGF agents on radio-induced OCTA features.

In this report, local fractal dimension was used to assess superficial and deep plexus disorganization in OCTA images. Fractal dimension has previously been used to investigate the retinal microvasculature in fundus^{49–52} or OCTA^{10,12,13} images. By evaluating pattern repetition at different scales,⁵³ fractal dimension is particularly adapted to assess the integrity of arborized vascular networks. However, the retinal vasculature does not follow a perfect fractal behavior at all scales. Therefore, the “local” fractal dimension, limiting the fractal analysis to a given scale range, as illustrated in Figures 1 and 2, may provide a reliable indicator of fractal behavior of the macular capillary network on OCTA.

This study had limitations, including its retrospective design and the use of the recent OCTA technology that lacks consensual terminology⁵⁴ and processing tools. Moreover, artifacts in OCTA acquisition and interpretation may alter the results, although low-quality images were discarded. Say et al.⁵⁵

have provided a comprehensive list of potential artifacts in OCTA imaging of irradiated eyes and shown that they were more frequent in eyes with worse visual function.

Overall, these results identified structural and microvascular factors contributing to the visual outcome of eyes with radiation maculopathy. Although FA remains the gold standard for the diagnosis and prognosis of radiation maculopathy, OCTA-derived quantitative metrics may offer promising tools. Future studies should evaluate the role of OCTA in predicting treatment response in radiation maculopathy.

Acknowledgments

The authors thank Marc Curchod and Laureen Vallat, MSc (Jules-Gonin Eye Hospital, Fondation Asile des Aveugles, Lausanne, Switzerland) for technical assistance; Alessia Pica, MD (Paul-Scherer Institute, Villigen, Switzerland) and Francine Behar-Cohen, MD, PhD (INSERM and Université Paris Descartes, Paris, France, and University of Lausanne, Switzerland) for fruitful discussions.

Supported by the Faculty of Biology and Medicine Research Commission Fund, University of Lausanne, Switzerland (AM).

Disclosure: A. Matet, None; A. Daruich, None; L. Zografas, None

References

1. Giuliani GP, Sadaka A, Hinkle DM, Simpson ER. Current treatments for radiation retinopathy. *Acta Oncol.* 2011;50:6–13.

2. Reichstein D. Current treatments and preventive strategies for radiation retinopathy. *Curr Opin Ophthalmol*. 2015;26:157-166.
3. Nagiel A, Sadda SR, Sarraf D. A promising future for optical coherence tomography angiography. *JAMA Ophthalmol*. 2015;133:629-630.
4. Jia Y, Bailey ST, Hwang TS, et al. Quantitative optical coherence tomography angiography of vascular abnormalities in the living human eye. *Proc Natl Acad Sci U S A*. 2015;112:E2395-E2402.
5. Hwang TS, Jia Y, Gao SS, et al. Optical coherence tomography angiography features of diabetic retinopathy. *Retina*. 2015;35:2371-2376.
6. Freiberg FJ, Pfau M, Wons J, Wirth MA, Becker MD, Michels S. Optical coherence tomography angiography of the foveal avascular zone in diabetic retinopathy. *Graefes Arch Clin Exp Ophthalmol*. 2016;254:1051-1058.
7. Agemy SA, Scripsma NK, Shah CM, et al. Retinal vascular perfusion density mapping using optical coherence tomography angiography in normals and diabetic retinopathy patients. *Retina*. 2015;35:2353-2363.
8. Shahlaee A, Samara WA, Hsu J, et al. In vivo assessment of macular vascular density in healthy human eyes using optical coherence tomography angiography. *Am J Ophthalmol*. 2016;165:39-46.
9. Gadde SGK, Anegondi N, Bhanushali D, et al. Quantification of vessel density in retinal optical coherence tomography angiography images using local fractal dimension. *Invest Ophthalmol Vis Sci*. 2016;57:246-252.
10. Zahid S, Dolz-Marcos R, Freund KB, et al. Fractal dimensional analysis of optical coherence tomography angiography in eyes with diabetic retinopathy. *Invest Ophthalmol Vis Sci*. 2016;57:4940-4947.
11. Bhanushali D, Anegondi N, Gadde SGK, et al. Linking retinal microvasculature features with severity of diabetic retinopathy using optical coherence tomography angiography. *Invest Ophthalmol Vis Sci*. 2016;57:519-525.
12. Kim AY, Chu Z, Shahidzadeh A, Wang RK, Puliafito CA, Kashani AH. Quantifying microvascular density and morphology in diabetic retinopathy using spectral-domain optical coherence tomography angiography. *Invest Ophthalmol Vis Sci*. 2016;57:OCT362-OCT370.
13. Kim AY, Rodger DC, Shahidzadeh A, et al. Quantifying retinal microvascular changes in uveitis using spectral-domain optical coherence tomography angiography. *Am J Ophthalmol*. 2016;171:101-112.
14. Shields CL, Say EAT, Samara WA, Khoo CTL, Mashayekhi A, Shields JA. Optical coherence tomography angiography of the macula after plaque radiotherapy of choroidal melanoma: comparison of irradiated versus nonirradiated eyes in 65 patients. *Retina*. 2016;36:1493-1505.
15. Veverka KK, Abouchehade JE, Iezzi R, Pulido JS. Noninvasive grading of radiation retinopathy the use of optical coherence tomography angiography. *Retina*. 2015;35:2400-2410.
16. Goitein M, Miller T. Planning proton therapy of the eye. *Med Phys*. 1983;10:275-283.
17. Moisy F. Boxcount: fractal dimension using the "box-counting" method for 1D, 2D and 3D sets. Available at: <https://ch.mathworks.com/matlabcentral/fileexchange/13063-boxcount/content/boxcount/html/demo.html>. Published 2008. Accessed March 18, 2017.
18. Cohen J. A coefficient of agreement for nominal scales. *Educ Psychol Meas*. 1960;20:37-46.
19. Venables WN, Ripley BD. *Modern Applied Statistics With S*. 4th ed. New York: Springer; 2002.
20. Patel AV, Lane AM, Morrison MA, et al. Visual outcomes after proton beam irradiation for choroidal melanomas involving the fovea. *Ophthalmology*. 2016;123:369-377.
21. Guyer DR, Mukai S, Egan KM, Seddon JM, Walsh SM, Gragoudas ES. Radiation maculopathy after proton beam irradiation for choroidal melanoma. *Ophthalmology*. 1992;99:1278-1285.
22. Gass JD. A fluorescein angiographic study of macular dysfunction secondary to retinal vascular disease, VI: X-ray irradiation, carotid artery occlusion, collagen vascular disease, and vitritis. *Arch Ophthalmol*. 1968;80:606-617.
23. Hayreh SS. Post-radiation retinopathy: a fluorescence fundus angiographic study. *Br J Ophthalmol*. 1970;54:705-714.
24. Brown GC, Shields JA, Sanborn G, Augsburger JJ, Savino PJ, Schatz NJ. Radiation retinopathy. *Ophthalmology*. 1982;89:1494-1501.
25. Say EAT, Samara WA, Khoo CTL, et al. Parafoveal capillary density after plaque radiotherapy for choroidal melanoma: analysis of eyes without radiation maculopathy. *Retina*. 2016;36:1670-1678.
26. Balaratnasingam C, Inoue M, Ahn S, et al. Visual acuity is correlated with the area of the foveal avascular zone in diabetic retinopathy and retinal vein occlusion. *Ophthalmology*. 2016;123:2352-2367.
27. Casselholmde Salles M, Kvanta A, Amréen U, Epstein D. Optical coherence tomography angiography in central retinal vein occlusion: correlation between the foveal avascular zone and visual acuity. *Invest Ophthalmol Vis Sci*. 2016;57:OCT242-OCT246.
28. Samara WA, Shahlaee A, Adam MK, et al. Quantification of diabetic macular ischemia using optical coherence tomography angiography and its relationship with visual acuity. *Ophthalmology*. 2016;124:235-244.
29. Samara WA, Shahlaee A, Sridhar J, Khan MA, Ho AC, Hsu J. Quantitative optical coherence tomography angiography features and visual function in eyes with branch retinal vein occlusion. *Am J Ophthalmol*. 2016;166:76-83.
30. Wakabayashi T, Sato T, Hara-Ueno C, et al. Retinal microvasculature and visual acuity in eyes with branch retinal vein occlusion: imaging analysis by optical coherence tomography angiography. *Invest Ophthalmol Vis Sci*. 2017;58:2087-2094.
31. Matet A, Daruich A, Dirani A, Ambresin A, Behar-Cohen F. Macular telangiectasia type 1: capillary density and microvascular abnormalities assessed by optical coherence tomography angiography. *Am J Ophthalmol*. 2016;167:18-30.
32. Adhi M, Filho MAB, Louzada RN, et al. Retinal capillary network and foveal avascular zone in eyes with vein occlusion and fellow eyes analyzed with optical coherence tomography angiography. *Invest Ophthalmol Vis Sci*. 2016;57:OCT486-OCT494.
33. Coscas F, Glacet-Bernard A, Miere A, et al. Optical coherence tomography angiography in retinal vein occlusion: evaluation of superficial and deep capillary plexa. *Am J Ophthalmol*. 2016;161:160-171.e2.
34. Rispoli M, Savastano MC, Lumbroso B. Capillary network anomalies in branch retinal vein occlusion on optical coherence tomography angiography. *Retina*. 2015;35:2332-2338.
35. Mané V, Dupas B, Gaudric A, et al. Correlation between cystoid spaces in chronic diabetic macular edema and capillary nonperfusion detected by optical coherence tomography angiography. *Retina*. 2016;36:S102-S110.
36. Spaide RF. Retinal vascular cystoid macular edema: review and new theory. *Retina*. 2016;36:1823-1842.
37. Couturier A, Mané V, Bonnin S, et al. Capillary plexus anomalies in diabetic retinopathy on optical coherence tomography. *Retina*. 2015;35:2384-2391.
38. Horgan N, Shields CL, Mashayekhi A, Shields JA. Classification and treatment of radiation maculopathy. *Curr Opin Ophthalmol*. 2010;21:233-238.
39. Engerman RL, Pfaffenbach D, Davis MD. Cell turnover of capillaries. *Lab Invest*. 1967;17:738-743.

40. Archer DB, Gardiner TA. Ionizing radiation and the retina. *Curr Opin Ophthalmol*. 1994;5:59–65.
41. Dimitrievich GS, Fischer-Dzoga K, Griem ML. Radiosensitivity of vascular tissue, I: differential radiosensitivity of capillaries: a quantitative in vivo study. *Radiat Res*. 1984;99:511–535.
42. Bonnin S, Mané V, Couturier A, et al. New insight into the macular deep vascular plexus imaged by optical coherence tomography. *Retina*. 2015;35:2347–2352.
43. Krema H, Xu W, Payne D, Maria Vasquez L, Pavlin CJ, Simpson R. Factors predictive of radiation retinopathy post 125Iodine brachytherapy for uveal melanoma. *Can J Ophthalmol*. 2011; 46:158–163.
44. Aziz HA, Singh N, Bena J, Wilkinson A, Singh AD. Vision loss following episcleral brachytherapy for uveal melanoma: development of a vision prognostication tool. *JAMA Ophthalmol*. 2016;134:615–620.
45. Vasa M, Breitschopf K, Zeiher AM, Dimmeler S. Nitric oxide activates telomerase and delays endothelial cell senescence. *Circ Res*. 2000;87:540–542.
46. Minamino T, Miyauchi H, Yoshida T, Ishida Y, Yoshida H, Komuro I. Endothelial cell senescence in human atherosclerosis. *Circulation*. 2002;105:1541–1544.
47. Mantel I, Schalenbourg A, Bergin C, Petrovic A, Weber DC, Zografos L. Prophylactic use of bevacizumab to avoid anterior segment neovascularization following proton therapy for uveal melanoma. *Am J Ophthalmol*. 2014;158:693–701.e2.
48. Kim IK, Lane AM, Jain P, Awh C, Gragoudas ES. Ranibizumab for the prevention of radiation complications in patients treated with proton beam irradiation for choroidal melanoma. *Trans Am Ophthalmol Soc*. 2016;114:T2.
49. Daxer A. Characterisation of the neovascularisation process in diabetic retinopathy by means of fractal geometry: diagnostic implications. *Graefes Arch Clin Exp Ophthalmol*. 1993;681–686.
50. Thomas GN, Ong SY, Tham YC, et al. Measurement of macular fractal dimension using a computer-assisted program. *Invest Ophthalmol Vis Sci*. 2014;55:2237–2243.
51. Cheung N, Donaghue KC, Liew G, et al. Quantitative assessment of early diabetic retinopathy using fractal analysis. *Diabetes Care*. 2009;32:106–110.
52. Williams MA, McGowan AJ, Cardwell CR, et al. Retinal microvascular network attenuation in Alzheimer's disease. *Alzheimers Dement (Amst)*. 2015;1:229–235.
53. Mandelbrot B. How long is the coast of Britain: statistical self-similarity and fractional dimension. *Science*. 1967;156:636–638.
54. Fawzi AA. Consensus on optical coherence tomographic angiography nomenclature. *JAMA Ophthalmol*. 2017;135: 377–378.
55. Say EAT, Ferenczy S, Magrath GN, Samara WA, Khoo CTL, Shields CL. Image quality and artifacts on optical coherence tomography angiography: comparison of pathologic and paired fellow eyes in 65 patients with unilateral choroidal melanoma treated with plaque radiotherapy [published online ahead of print November 23, 2016]. *Retina*. doi:10.1097/IAE.0000000000001414.